IEEE Photonics Journal
An IEEE Photonics Society Publication

Open Access

Filter-Free Photonic Image-Rejection Down-Conversion for Distributed Antenna Applications

Volume 13, Number 2, April 2021

Dayong Wang
Feng Yang
Yunxin Wang
Zhiyu Chen
Dengcai Yang
Fuzheng Wu

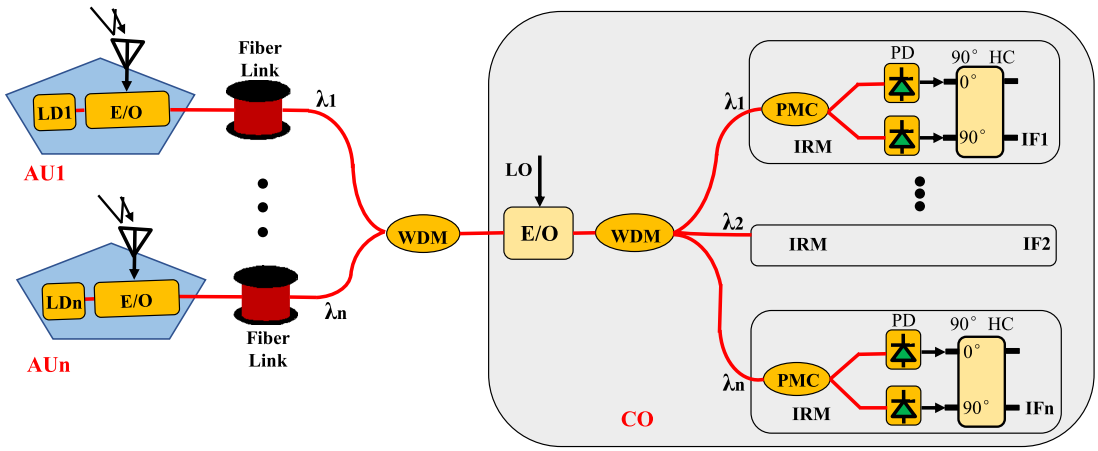

DOI: 10.1109/JPHOT.2021.3064553

Filter-Free Photonic Image-Rejection Down-Conversion for Distributed Antenna Applications

Dayong Wang,[1,2] Feng Yang,[1,2] Yunxin Wang,[1,2] Zhiyu Chen,[3] Dengcai Yang,[4] and Fuzheng Wu[4]

[1]The College of Physics and Optoelectronics, Faculty of Science, Beijing University of Technology, Beijing 100124, China
[2]Beijing Engineering Research Center of Precision Measurement Technology and Instruments, Beijing University of Technology, Beijing 100124, China
[3]Science and Technology on Electronic Information Control Laboratory, Chengdu 610036, China
[4]Institute of Advanced Technology on Semiconductor Optics & Electronics, Institute of Laser Engineering, Beijing University of Technology, Beijing 100124, China

DOI:10.1109/JPHOT.2021.3064553
This work is licensed under a Creative Commons Attribution 4.0 License. For more information, see https://creativecommons.org/licenses/by/4.0/

Manuscript received February 5, 2021; revised February 28, 2021; accepted March 2, 2021. Date of publication March 8, 2021; date of current version March 29, 2021. This work was supported in part by the Beijing Natural Science Foundation under Grant 4202001, in part by the National Natural Science Foundation of China under Grants 61771438 and 61871007, and in part by the National Key Research and Development Project (2020YFB2205700). Corresponding author: Yunxin Wang (e-mail: yxwang@bjut.edu.cn).

Abstract: Photonics-assisted frequency conversion based on cascaded modulators is an effective way to satisfy the requirements of distributed antenna array applications. A filter-free photonic image-rejection down-converter with immunity to dispersion-induced power fading is proposed and demonstrated. The radio frequency (RF) signal from the distributed antenna unit is injected into a dual-drive Mach–Zehnder modulator (DDMZM) through an electrical 90° hybrid coupler (HC), and a single-sideband (SSB) signal is realized. It is then transmitted to the center office by an optical fiber link. At the center office, the modulated RF signal is injected into a dual-polarization dual-parallel MZM (DP-DPMZM) after a polarization controller (PC). Afterwards, an LO signal remodulates it through the Y-DPMZM, and carrier-suppressed SSB modulation is fulfilled via another electrical 90° HC. After the power splitting, quadrature I and Q IF signals can be obtained by a photonics-based continuously adjustable phase shifter. Through a combination of the I/Q IF signals with a low-frequency electrical 90° HC, a photonics image-rejection down-converter based on phase cancellation is realized. Moreover, no optical filter is required; thus, the image-rejection down-converter can work with a large bandwidth. The proposed filter-free photonic image-rejection down-converter is theoretically analyzed and experimentally verified.

Index Terms: Microwave photonics, distributed antenna, image rejection, photonic down-conversion.

1. Introduction

Microwave photonic links (MPLs) have significant advantages, i.e., low transmission loss, good flexibility, broad bandwidth, and non-sensitivity to electromagnetic disturbances, and they have recently been deeply explored and rapidly promoted [1]. Microwave photonics frequency down-conversion can effectively ease the bandwidth demand of the follow-up ADC processing. Owing to the low-loss

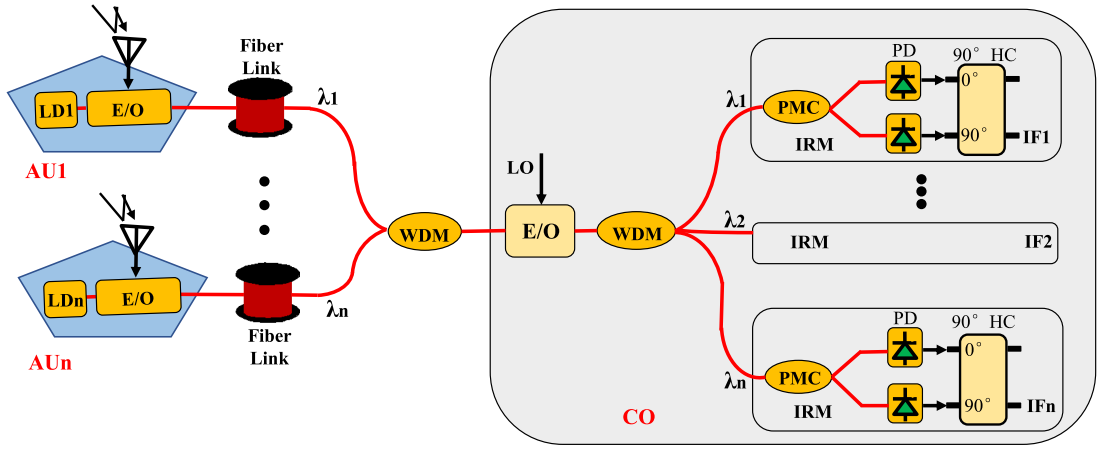

Fig. 1. Diagram of a distributed antenna system. LD: Laser diode; E/O: electrical-to-optical conversion; WDM: wavelength demultiplexer; LO: local oscillation; CO: center office; AU: antenna unit; IRM: image-rejection mixer; PMC: polarization maintaining coupler; PD: photodetector; HC: hybrid coupler; IF: intermediate frequency.

characteristic in fiber-based long-distance transmission, the photonics-assisted downconverter has become one of the most important elements in distributed antenna array applications [2], such as radio-over-fiber (RoF), phase-coded radar systems, beamforming networks, cellular wireless networks, and remote sensing [1]–[5].

To simplify the architecture of the down-conversion module, many photonics frequency converters [6]–[14] are incorporated into a single integrated modulator. Therefore, local oscillator (LO) and radio frequency (RF) signals are required to modulate the same electro-optic modulator. However, this kind of down-converter is not suitable for the distributed antenna application as shown in Fig. 1. To reduce the complexity of the distributed antenna unit (AU), multiple AUs contribute to the receiving and electro-optic (EO) transform of the RF signal. Then the down-conversion and other processes are realized in the center office (CO) with the same LO signal to facilitate the dynamic allocation and control of radio resources. In this situation, the LO and RF signals have to carry out EO modulation at different locations. Each AU uses a distinctive optical carrier to transmit the RF signal. At CO, a single EO modulator is applied to load the LO signal and generate optical sidebands of LO signal. Finally, the signal from each AU is processed independently after a wavelength demultiplexer (WDM). Naturally, high isolation between the RF and LO signals can also be supplied within a wide operation bandwidth.

An image signal (IM) lying at another side of the LO signal might produce in-band image interference, which will deteriorate the down-converted signal [15]–[18]. The image-rejection frequency conversion with separated LO and RF modulation has been investigated by using parallel or cascaded structures. Several mixers with a 90° optical hybrid have been proposed [19]–[22]. The LO and RF signals are fed into two parallel branches. However, in a coherent receiver system, the phase instability of two independent branches influences the long-distance transmission.

Many image-rejection down-converters based on cascaded modulators and phase cancellation have been proposed by using Hartley structure [23]–[29]. A dual-parallel Mach–Zehnder modulator (DPMZM) and a MZM with individual transfer features are cascaded for two perpendicular polarized light waves [23]. However, the amount of fast-axis light lost is only approximately 15 dB, which may cause residual polarization of the RF signal. Moreover, image rejection has not been verified experimentally. For image rejection in down-conversion, introducing the quadrature phase difference between the target RF and IM down-converted signals is crucial for phase cancellation. This quadrature phase shift can be generated by an electrical hybrid coupler (HC) [24], [25]. Phase modulators (PMs) are cascaded to realize down-conversion in heterodyne image rejection [24]. In this scheme, one PM is used to modulate the RF signal, and two parallel PMs are applied to

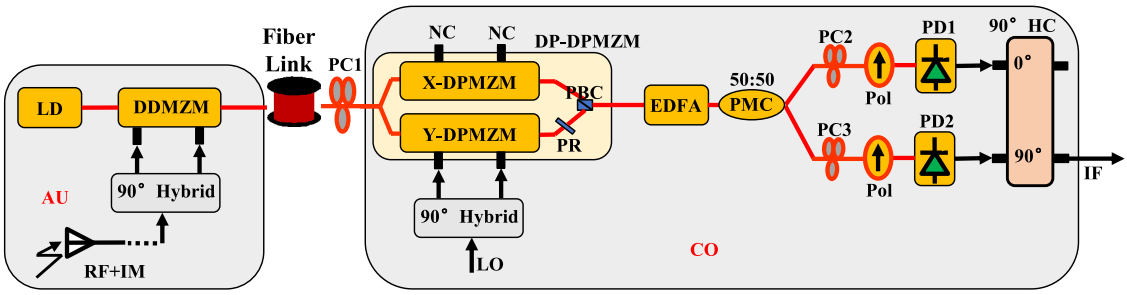

Fig. 2. Schematic diagram of the proposed photonic image-rejection down-conversion. DDMZM: dual-drive Mach–Zehnder modulator; PC: polarization controller; Pol: polarizer; DP-DPMZM: dual-polarization dual-parallel MZM; PR: polarization rotator; PMC: polarization maintaining coupler; EDFA: erbium-doped fiber amplifier; PD: photodetector; HC: hybrid coupler; CO: center office; AU: antenna unit.

suppress the mirror signal by an electrical HC, which makes the system complicated. Photonic down-conversion is implemented based on a MZM in tandem with a dual-polarization MZM [25], and here, the quadrature phase is induced by an electrical 90° HC relative to the LO signal. Nevertheless, the electrical 90° hybrid is frequency dependent, and it cannot maintain a precise 90° phase difference within a wide bandwidth. Moreover, the double-sideband (DSB) modulation of the MZM suffers from chromatic-dispersion-induced power fading in antenna remoting applications. To broaden the bandwidth of image rejection, a photonic-assisted phase shift has also been adopted. The phase shift can be controlled by a polarization controller (PC) in combination with orthogonal polarization signals. A photonic-based image-rejection down-converter for fiber remoting has been investigated by using a PM and a polarization modulator (PolM) [26]. The subsequent digital processing is carried out to further optimize the phase and amplitude balances between the I and Q intermediate frequency (IF) signals, resulting in good image rejection. Image-rejection down-conversion has been realized by two reversed-series PMs in a Sagnac loop [27], in which the LO and RF modulations are distinguished based on the velocity mismatch of the PM at high frequency. In addition, the phase shift can be generated by bias voltage adjustment of the modulators. The cascaded PM and a DPMZM [28] or a dual-drive Mach-Zehnder modulator (DDMZM) [29] have been designed for image-rejection down-conversion and fiber remoting. In these methods, a WDM is used to remove the optical carrier and uncouple the upper and lower sidebands; thus, the lowest working frequency of the converters is constrained by the roll-off coefficient of the WDM.

In this paper, filter-free photonic image-rejection down-conversion with immunity to dispersion-induced power fading is proposed and verified for distributed antenna applications. In the proposed scheme, the distributed antenna units and central office are located at different places, and the RF signal is transported by a fiber-optic link. The RF signal is injected into a dual-drive Mach–Zehnder modulator via an electrical 90° HC, and single-sideband (SSB) modulation of the RF signal is realized. At the CO, this RF modulation signal is fed to a dual-polarization DPMZM (DP-DPMZM) after a PC. Then, the LO signal is input into the Y-DPMZM, and carrier-suppressed SSB (CS-SSB) modulation is fulfilled through an electrical 90° HC. After the power splitting, the I and Q IF signals are finally obtained by independent polarization adjustment. With the use of a low-frequency electrical 90° HC, a photonics image-rejection down-converter based on phase cancellation is achieved. No optical filter is needed in the link; thus, the image-rejection down-converter can work at a lower frequency. Because only the single sideband of the RF signal is acquired in the AU, the issue of chromatic dispersion is intrinsically settled.

2. Topology and Operation Principle

The image-free frequency down-converter for distributed antenna applications is schematically illustrated in Fig. 2. The optical carrier emitted from a laser is injected into a DDMZM. The useful

RF signal and image signal received by an antenna are fed to the DDMZM through an electrical 90° HC. Then, the RF-modulated signal enters a DP-DPMZM, which is made of two sub-DPMZMs in parallel paths, and a 90° polarization rotator (PR) is located after the Y-DPMZM. An LO signal is fed into the Y-DPMZM through another electrical 90° HC to complete the CS-SSB modulation. Therefore, the RF and LO signals are modulated at different polarization states. An erbium-doped fiber amplifier (EDFA) is inserted to compensate for the system loss. After a polarization maintaining coupler (PMC), the amplified signal is sent to two arms, each with a PC and a polarizer (Pol). By changing PC2 and PC3, a 90° phase shift is formed relative to the IF signal obtained by PD1 and PD2, and the quadrature IF signal is obtained. Finally, a low-frequency electrical 90° HC is used to unite the two quadrature IF signals, and image-reject down-conversion is implemented.

The output of the laser diode can be expressed as $E_{in}(t) = E_0 \exp(j\omega_c t)$, where E_0 and ω_c are its amplitude and angular frequency, respectively. Under the assumption that the initial RF phase is zero, the RF signal can be denoted by $V_{RF}\cos(\omega_{RF}t)$, where V_{RF} and ω_{RF} are the amplitude and angular frequency, respectively. To achieve RF SSB modulation, the DDMZM modulator works at the quadrature transmission point (QTP). In the small-signal approximation, the high-order modulations (n $\geq$ 2) are neglected. Then, the output of the DDMZM can be expanded according to the Bessel function and represented as

$$E_{DDMZM}(t) \approx \frac{1}{2}E_0\left[J_0(m_{RF})\cos(\omega_0 t) + J_1(m_{RF})\cos(\omega_0 - \omega_{RF})t\right] \tag{1}$$

where $m_{RF} = \pi V_{RF}/V_\pi$ is the modulation depth of the DDMZM and V_π is the half-wave voltage of the DDMZM. $J_n(\bullet)$ is the nth-order Bessel function of the first kind.

The RF-modulated signal is input to the DP-DPMZM. To ensure that this signal passes directly through the X-DPMZM, the lower sub-MZM must be set to the null transmission point (NTP). At the same time, the upper and main sub-MZMs should be tuned to the maximum transmission point (MTP). The LO signal is transmitted into the Y-DPMZM via an electrical 90° HC. To achieve CS-SSB modulation, both the upper and lower sub-MZMs must be maintained at the NTP, and the main sub-MZM must be regulated to the quadrature point. In other words, $\theta_4 = \theta_5 = \pi$ and $\theta_6 = \pm\pi/2$ should be met. Here, $\theta_6 = +\pi/2$ is set to obtain the -1st-order modulation sideband of the LO signal. Under the small-signal approximation, the modulation of the LO signal to the -1st-order RF modulation signal can be ignored. If the initial LO phase is zero, the output of the Y-DPMZM can be written as

$$E_{Y-DPMZM}(t) \approx \frac{\sqrt{2}}{4}E_0\left[J_0(m_{RF})J_1(m_{LO})\cos(\omega_0 - \omega_{LO})t\right] \tag{2}$$

where $m_{LO} = \pi V_{LO}/V_{\pi 1}$ is the modulation depth of the Y-DPMZM and $V_{\pi 1}$ is the half-wave voltage of the two DPMZMs in the DP-DPMZM. $\theta_n = \pi V_{bn}/V_{\pi 1}$ (n = 1, 2 …, 6) is the phase difference produced by the bias voltage.

Then, the optical distribution of the DP-DPMZM can be denoted by

$$\begin{aligned} E_{DP-DPMZM}(t) &= [E_X, E_Y] \\ &\approx \frac{\sqrt{2}}{4}E_0\left[J_0(m_{RF})\cos(\omega_0 t) + J_1(m_{RF})\cos(\omega_0 - \omega_{RF})t,\ J_0(m_{RF})J_1(m_{LO})\cos(\omega_0 - \omega_{LO})t\right] \end{aligned} \tag{3}$$

After the EDFA, the amplified signal is divided into two channels (I and Q) by a PMC. Each channel is followed by a PC and a Pol to realize a photonic phase shift. By adjusting the PCs, we cause the axes to form a 45° polarization angle between the DP-DPMZM modulator and the Pol. The transformation matrix of the PC is

$$T = \frac{\sqrt{2}}{2}\begin{bmatrix} 1 & -\exp(j\phi) \\ \exp(j\phi) & 1 \end{bmatrix} \tag{4}$$

where ϕ is the phase difference between the X and Y polarization states induced by the PC.

The outputs of channel I and channel Q are detected by the PDs and can be written as

$$I_{Channel-I}(t) \propto \Re\left[J_0(m_{RF})J_1(m_{RF})J_1(m_{LO})\cos\left(\omega_{RF}t-\omega_{LO}t-\phi_I\right)\right] \tag{5}$$

$$I_{Channel-Q}(t) \propto \Re\left[J_0(m_{RF})J_1(m_{RF})J_1(m_{LO})\cos\left(\omega_{RF}t-\omega_{LO}t-\phi_Q\right)\right] \tag{6}$$

It can be seen that the phase of the down-converted IF signals (channels I and Q) can be independently and continuously adjusted through the PC. To achieve image rejection, the two channels should be quadrature. Then, let $\phi_I = 0$ and $\phi_Q = \pi/2$; thus, the output of the PDs can be formulated as

$$I_{Channel-I}(t) \propto \Re\left[J_0(m_{RF})J_1(m_{RF})J_1(m_{LO})\cos\left(\omega_{RF}t-\omega_{LO}t\right)\right] \tag{7}$$

$$I_{Channel-Q}(t) \propto \Re\left[J_0(m_{RF})J_1(m_{RF})J_1(m_{LO})\sin(\omega_{RF}t-\omega_{LO}t)\right] \tag{8}$$

The image signal is loaded accompanied by the useful RF signal, it is also transmitted in the proposed schema. The output of the PDs can be rewritten as

$$I_{Channel-I}(t) \propto \Re\left[J_0(m_{RF})J_1(m_{RF})J_1(m_{LO})\cos(\omega_{RF}t-\omega_{LO}t)+J_0(m_{IM})J_1(m_{IM})J_1(m_{LO})\cos(\omega_{LO}t-\omega_{IM}t)\right] \tag{9}$$

$$I_{Channel-Q}(t) \propto \Re\left[J_0(m_{RF})J_1(m_{RF})J_1(m_{LO})\sin(\omega_{RF}t-\omega_{LO}t)-J_0(m_{IM})J_1(m_{IM})J_1(m_{LO})\sin(\omega_{LO}t-\omega_{IM}t)\right] \tag{10}$$

Finally, an electrical 90° HC is used to combine these two channels to eliminate the image signal, which can be expressed as

$$\begin{aligned} I(t) \propto\ & \Re J_0(m_{RF})J_1(m_{RF})J_1(m_{LO})\left[\cos(\omega_{RF}t-\omega_{LO}t)+\sin\left(\omega_{RF}t-\omega_{LO}t+\pi/2\right)\right] \\ & + \Re J_0(m_{IM})J_1(m_{IM})J_1(m_{LO})\left[\cos(\omega_{LO}t-\omega_{IM}t)-\sin\left(\omega_{LO}t-\omega_{IM}t+\pi/2\right)\right] \\ & = 2\Re J_0(m_{RF})J_1(m_{RF})J_1(m_{LO})\cos(\omega_{RF}-\omega_{LO})t \end{aligned} \tag{11}$$

It is understandable that the image signal at $\omega_{LO}-\omega_{IM}$ is rejected and that the desired down-converted RF signal at $\omega_{RF}-\omega_{LO}$ is enhanced by 3 dB. Owing to the cascaded modulation, the RF signal and LO source can be placed at different locations for the distributed antenna array scenario. Owing to the photonic-based phase shifter, the I/Q signals can be made quadrature with frequency independence. Because of the lack of an optical filter, the image-rejection down-converter can also work at a lower frequency. Hence, the proposed method possesses a wide operation bandwidth. Thanks to the SSB modulation of the RF signal in the AU, chromatic dispersion introduced by the long-distance transmission can be suppressed. Furthermore, the modulators are operated at the normal points; thus, commercial bias controllers can be used in the proposed MPL to achieve stable long-distance transmission.

3. Experimental Results

The proposed frequency down-converter shown in Fig. 2 is utilized. An optical carrier from a continuous wave laser (Emcore, TTX1994) with a power of 16 dBm and wavelength of 1549.99 nm is injected into the DDMZM (Fujitsu, FTM7937EZ), and the half-wave voltage is 3.5 V for a single-end drive. An RF signal launched from an analog signal source (Rohde & Schwarz SMB100A) is applied to the two radio ports via an electrical 90° HC (Marki Microwave QH-0226, 2-26.5 GHz). The DDMZM works at Quad+ to obtain the -1st-order optical sideband of the RF signal. Then, it is transmitted through a 1-km single-mode fiber (SMF) to the center unit. A PC is also used to avoid polarization-dependent loss before the DP-DPMZM. An LO signal supplied by a microwave signal generator (Agilent, 8257D) is applied to the Y-DPMZM of the DP-DPMZM (Fujitsu, FTM7977HQA) via an electrical 90° HC, and the half-wave voltage of the DP-DPMZM is approximately 3.5 V. An EDFA is adopted to improve the optical power. After that, a PMC is used to split the power, two PCs and two Pols are then used to generate a pair of quadrature IF signals. Finally, a low-frequency electrical 90° HC (MECA, 3dB 90° HYBRID COUPLER, 705S-1.700V) is used to incorporate the

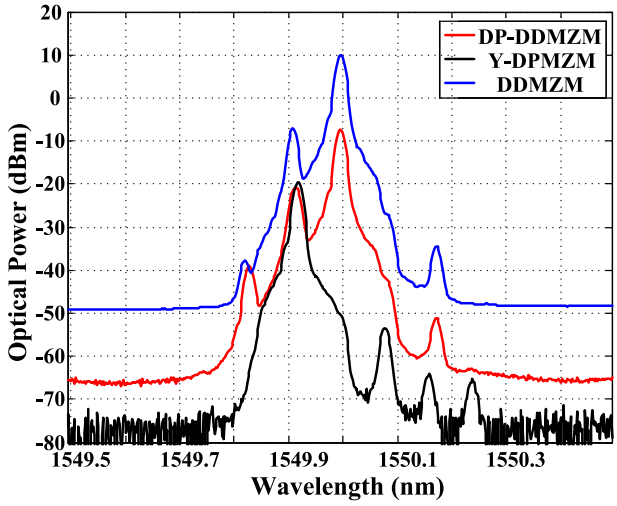

Fig. 3. Measured optical spectra of the output of the DDMZM (blue line), the output of the Y-DPMZM without an RF signal (black line), and the output of the DP-DPMZM with both RF and LO signals (red line).

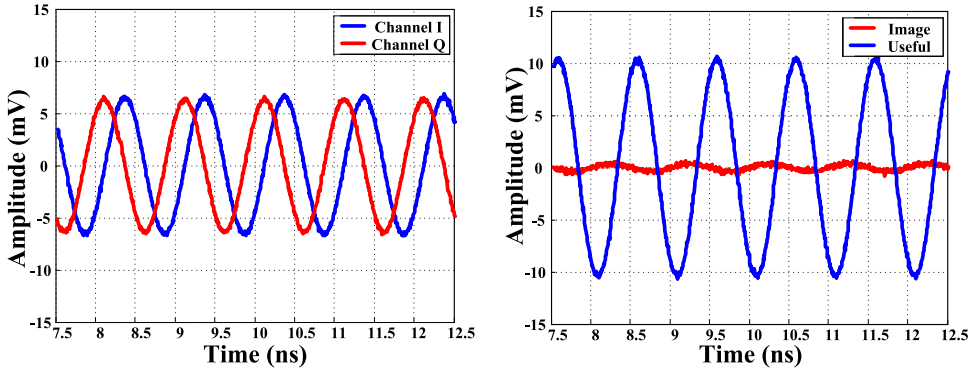

Fig. 4. Measured waveforms of the I and Q IF signals converted from the useful signal. (a) the image signal (b) and the output of the HC with both useful and image signals at the same time.

IF signals from the two single-ended mixers, and the photonics image-rejection down-converter based on phase cancellation is implemented.

In the experiments, the frequency and power of the RF signal are 11 GHz and 0 dBm, respectively, and those of the LO signal are 10 GHz and 5 dBm. The optical spectra are obtained by an optical spectrum analyzer (OSA, Yokogawa, AQ6370C), as shown in Fig. 3. The blue line illustrates the SSB modulation after the DDMZM. The black line shows the CS-SSB modulation via the Y-DPMZM without the RF signal in the DDMZM. When both the RF and LO signals modulate the DDMZM and Y-DPMZM, the output spectrum of the DP-DPMZM is marked by the red line. It is difficult to distinguish the RF and LO sidebands due to the limited resolution of the OSA (0.02 nm).

According to (7) and (8), the IF signals in channels I and Q should be quadrature for image rejection. To meet this condition, the waveforms of the two channels are measured by a multichannel oscilloscope (MSO6104A), and the results are represented in Fig. 4(a). We can see that their phase difference can be adjusted to 90° accurately. The frequency and power of the image signal are 9 GHz and 0 dBm, respectively; thus, the useful and interferential IF signals are both at 1 GHz. These two IF waveforms are detected as shown in Fig. 4(b). The amplitude of the down-converted image signal is almost zero while the down-converted useful signal is enhanced in comparison with the single channel down-converted signal in Fig. 5(a). The two down-converted output IF signals of

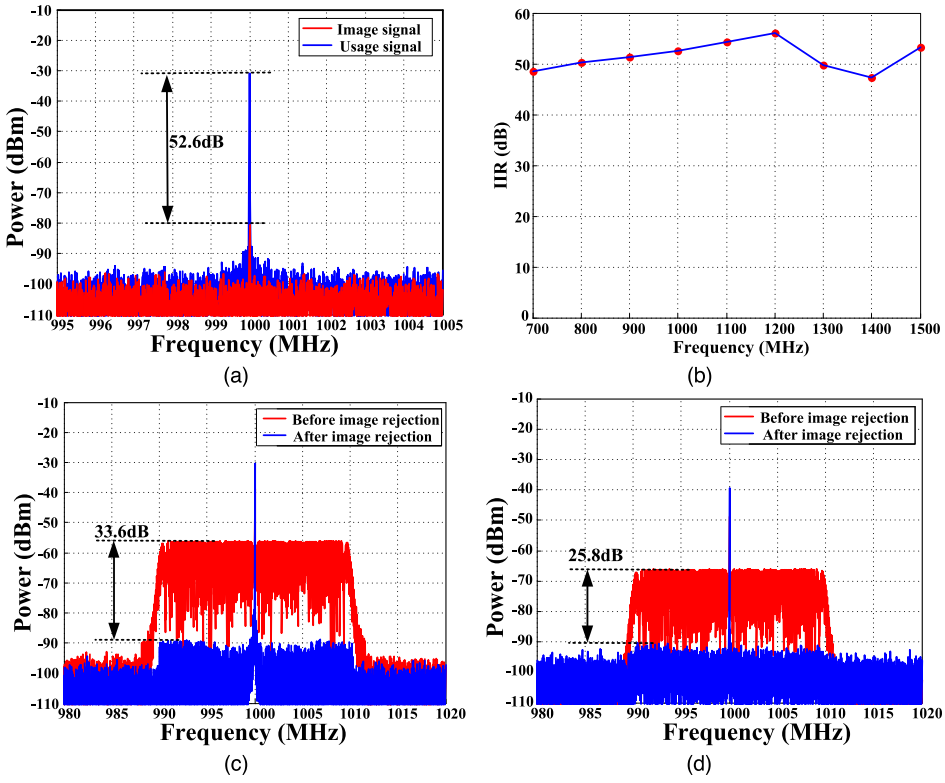

Fig. 5. Measured spectra of the down-converted IF signals. (a) A single-tone image signal, (b) measured IRRs for different frequencies of IF signal, (c) a broadband image signal after 1-km transmission, and (d) a broadband image signal after 25-km transmission.

the useful and image signals are also measured by an electrical spectrum analyzer (ESA, Keysight N9030B), and the result is shown in Fig. 5(a). It can be seen that the image-rejection ratio (IRR) reaches 52.6 dB in the single-tone case. Then, we keep the LO frequency at 10 GHz and change the RF from 10.7 to 11.5 GHz with a frequency interval of 100 MHz. The IRRs of different IF signals are shown in Fig. 5(b), and it can be seen that all of the IRRs are above 47.3 dB.

To verify the performance of broadband image suppression, the image signal is changed into a linear frequency modulation signal with a 9-GHz central frequency and a 20-MHz bandwidth. The down-converted output IF signals of the useful and image signals are shown in Fig. 5(c). Compared with the I and Q IF signals combined by a traditional 3-dB coupler and a 90° HC, the SNR is increased by 33.6 dB after the image rejection operation. Furthermore, to estimate the capability of long-distance transmission, the length of the SMF is increased to 25 km. The spectra of image rejection are shown in Fig. 5(d). It can be found that the power level of the useful IF signal linearly decreases due to the linear loss in fiber transmission. The SNR is improved by 25.8 dB. Therefore, an EDFA is inserted before the PMC to compensate for the loss. The auto-control loop of power and phase with electric optical attenuator and electric polarization controller can be used to compensate the balance of I and Q channel, which can also improve the reliability and stability of the proposed image-reject down-converter [27].

The phase noises of the down-converted signals with image rejection are also evaluated. For transmission over a distance of 1-km, the phase noises of LO, RF, and IF signals are measured, as shown in Fig. 6(a). The performance of the photonics-based converter depends mainly on the noise level of the LO and RF signals. Fig. 6(b) illustrates the phase noise of the down-converted signals under 1-km and 25-km fiber transmissions. We can see that the phase noise is nearly unchanged at the lower offset.

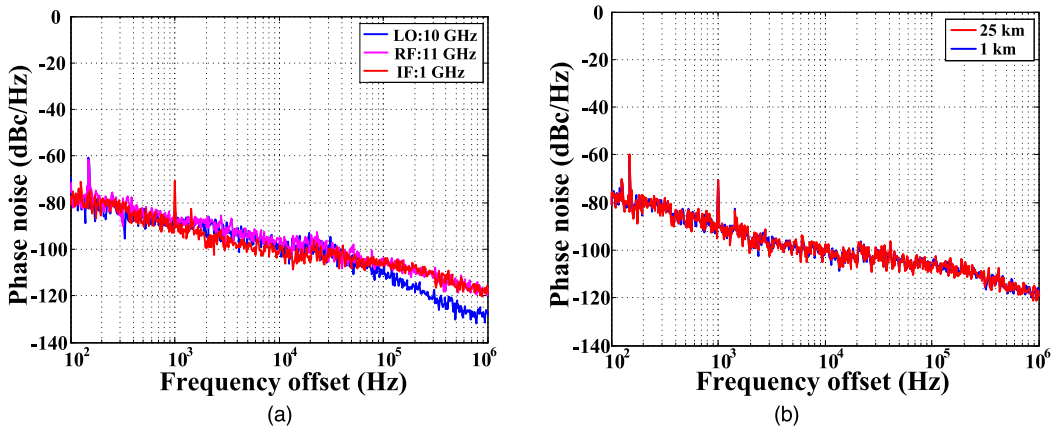

Fig. 6. Measured phase noises of (a) LO, RF, and IF signals for a 1-km transmission and (b) IF signals for different transmission lengths.

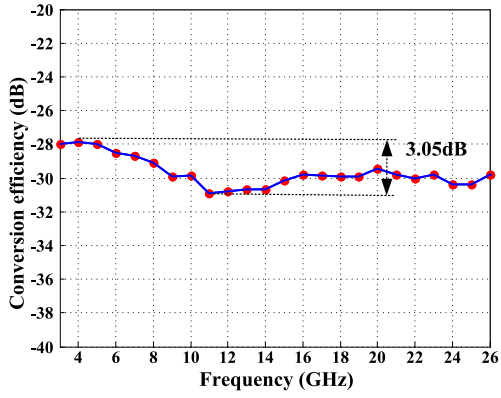

Fig. 7. Measured conversion efficiency of down-converted IF signals under different RF frequencies.

Due to the limitation of the electrical 90° HCs in our laboratories, only a frequency range of 3-26 GHz was evaluated. Fig. 7 depicts the conversion efficiency for RF frequencies from 3 GHz to 26 GHz. There is no optical filter in the offered MPL; thus, the operation frequency can be as low as 3 GHz. Keeping the down-converted IF signal unchanged at 1 GHz, the conversion efficiency of the down-converter is -29.37 ± 1.52 dB, and the peak-to-peak value is 3.05 dB. It can be observed that the conversion efficiency is much flatter within 23 GHz. Commercial HCs with bandwidths larger than 50 GHz are widely used. Therefore, the bandwidth of the proposed system can be improved to more than 40 GHz.

The chromatic dispersion compensation ability of the proposed cascaded link is analyzed. In the experiment, the response of the down-converter cannot be directly measured by a vector network analyzer (VNA). Therefore, an electric mixer is used to recover the converted signal. A test system as shown in Fig. 8(a) is built to analyze the frequency response of the down-converter with a VNA. An electrical coupler is used to split the LO signal from signal generator (Rohde & Schwarz SMB100A) into two parts. One part is used to the proposed link, and the other one is injected into the electrical mixer, which is used to recovery the RF signal from VNA. In this way, we can measure the response of the down-converter with VNA. The LO signal is fixed at 9 GHz, and the RF signal from the VNA (Rohde & Schwarz ZNB40) is tuned from 10 GHz to 26 GHz. The powers of the RF and LO signals are 0 dBm and 8 dBm. For the sake of comparison, a down-conversion link based on double sideband (DSB) modulation is also established at the same transmission distance. The measured frequency responses of two links have been normalized, and the results are shown in

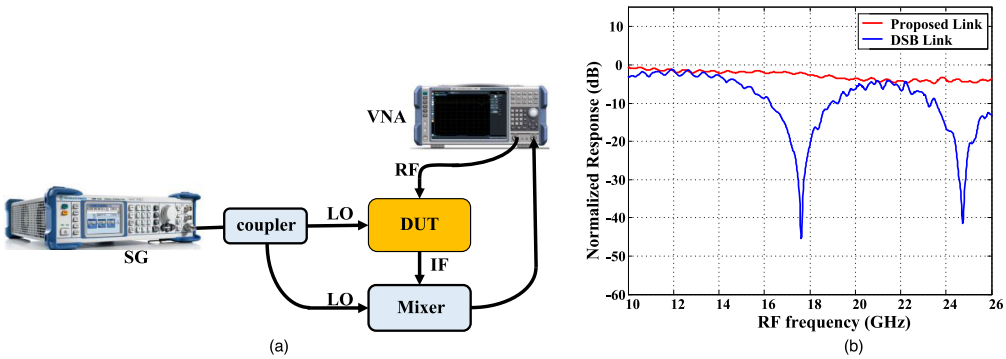

Fig. 8. (a) The experimental schematic diagram; (b) The frequency response of the DSB-based link and proposed link for a transmission distance of 25 km. SG: signal generator; DUT: device under testing; VNA: vector network analyzer.

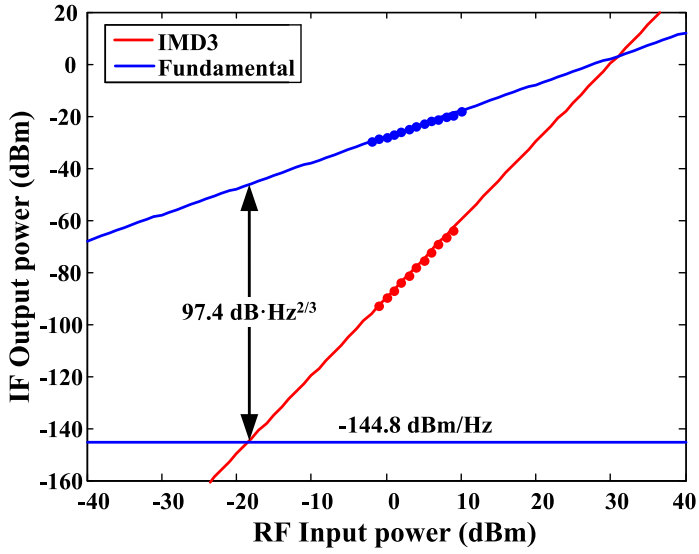

Fig. 9. SFDR of the proposed conversion method.

Fig. 8(b). In the DSB based link, the response of RF signal suffers different degrees of power fading with the change of frequency. However, in the proposed link, the response of RF signal is relatively flat. Therefore, due to the SSB modulation of RF signal, the power fading caused by dispersion can be well compensated for.

Finally, the spurious free dynamic range (SFDR) of the converter is measured. A two-tone RF signal at 11 GHz and 11.01 GHz is produced by analog signal sources (Rohde & Schwarz SMB100A). When the frequency and power of the LO signal are 10 GHz and 5 dBm, the power of the fundamental terms at 1 GHz and 1.01 GHz and the 3rd-order intermodulation distortions (IMD3) at 0.99 GHz and 1.02 GHz are measured by an ESA under different input RF powers. Fig. 9 indicates that the SFDR of the proposed converter is 97.4 dB·Hz$^{2/3}$.

4. Conclusion

A filter-free photonic image-rejection down-converter with immunity to dispersion-induced power fading is proposed and demonstrated to meet the demand of distributed antenna array applications. The photonic-based phase shifter can be precisely adjusted to 90° in a frequency-independent manner, which contributes to high image-rejection suppression. The downconverter without an

optical filter can work at a lower frequency. In view of the SSB modulation of the RF signal in the AU, chromatic dispersion can be reduced. Furthermore, the modulators are all operated at the normal points; thus, commercial bias controllers can be used in the proposed MPL to acquire long-term and steady transmission. The experimental results show that an IRR over 52.6 dB is achieved with a single-tone signal. For a broadband image signal, the SNR improves by 33.6 dB with image rejection. The RF bandwidth covers 3 to 26 GHz, with a very flat conversion efficiency. The proposed down-conversion method with image rejection has potential applications in distributed antenna arrays, microwave and millimeter wave receivers, and phase-coded radar systems.

References

[1] R. A. Minasian *et al*., "Microwave photonic signal processing," *Opt. Exp*., vol. 21, no. 19, pp. 22918–22936, Sep. 2013.
[2] Z. Tang *et al*., "Photonics-based microwave frequency mixing: Methodology and applications," *Laser Photon. Rev*., vol. 14, no. 1, pp. 1–25, Nov. 2019.
[3] J. Capmany *et al*., "Microwave photonic signal processing," *J. Lightw. Technol*., vol. 31, no. 4, pp. 571–586, Feb. 2013.
[4] M. Li *et al*., "Reconfigurable single-shot incoherent optical signal processing system for chirped microwave signal compression," *Sci. Bull*., vol. 62, no. 4, pp. 242–248, Feb. 2017.
[5] Z. Cao, X. Zhao, F. M. Soares, N. Tessema, and A. M. J. Koonen, "38-GHz millimeter wave beam steered fiber wireless systems for 5G indoor coverage: Architectures, devices, and links," *IEEE J. Quantum Electron*., vol. 53, no. 2, pp. 1–9, Feb. 2017.
[6] F. Yang *et al*., "Photonics-assisted frequency up/down conversion with tunable OEO and phase shift," *J. Lightw. Technol*., vol. 38, no. 23, pp. 6446–6457, Dec. 2020.
[7] T. Jiang *et al*., "Microwave photonic phase-tunable mixer," *Opt. Exp*., vol. 25, no. 4, pp. 4519–4527, Feb. 2017.
[8] F. Yang *et al*., "A microwave photonic phase-tunable mixer with local oscillator frequency doubling," *Opt. Commun*., vol. 438, pp. 141–146, May 2019.
[9] T. Li, E. H. W. Chan, X. Wang, X. Feng, B. Guan, and J. Yao, "Broadband photonic microwave signal processor with frequency up/down conversion and phase shifting capability," *IEEE Photon. J*., vol. 10, no. 1, Feb. 2018, Art. no. 5500112.
[10] Y. Wang *et al*., "All-optical microwave photonic downconverter with tunable phase shift," *IEEE Photon. J*., vol. 9, no. 6, Dec. 2017, Art. no. 5503408.
[11] Y. Gao *et al*., "Simultaneously photonic frequency downconversion, multichannel phase shifting, and IQ demodulation for wideband microwave signals," *Opt. Lett*., vol. 41, no. 19, pp. 4484–4487, Oct. 2016.
[12] W. Zhai *et al*., "A multi-channel phase tunable microwave photonic mixer with high conversion gain and elimination of dispersion-induced power fading," *IEEE Photon. J*., vol. 10, no. 1, Feb. 2018, Art. no. 5500210.
[13] M. Xie *et al*., "Anti-dispersion phase-tunable microwave mixer based on a dual-drive dual-parallel Mach-Zehnder modulator," *Opt. Exp*., vol. 26, no. 1, pp. 454–462, Jan. 2018.
[14] J. Zhang *et al*., "High-isolation microwave photonic sub-harmonic mixer," in *Proc. Int. Topical Meeting Microw. Photon*., Beijing, 2017, pp. 1–4.
[15] D. Zhu and S. Pan, "Photonics-based microwave image-reject mixer," *Photonics*, vol. 5, no. 6, pp. 1–12, Mar. 2018.
[16] Z. Tang and S. Pan, "Image-reject mixer with large suppression of mixing spurs based on a photonic microwave phase shifter," *J. Lightw. Technol*., vol. 34, no. 20, pp. 4729–4735, Oct. 2016.
[17] W. Zhang, A. Wen, E. H. W. Chan, X. Wang, X. Feng, and B. Guan, "Large bandwidth photonic microwave image rejection mixer with high conversion efficiency," *IEEE Photon. J*., vol. 9, no. 3, Jun. 2017, Art. no. 7201908.
[18] Z. Tang and S. Pan, "Reconfigurable microwave photonic mixer with minimized path separation and large suppression of mixing spurs," *Opt. Lett*., vol. 42, no. 1, pp. 33–36, Jan. 2017.
[19] S. Pan and Z. Tang, "A highly reconfigurable photonic microwave frequency mixer," *SPIE Newsroom*, pp. 1–3, 2015.
[20] Z. Meng *et al*., "Dual-band dechirping LFMCW radar receiver with high image rejection using microwave photonic I/Q mixer," *Opt. Exp*., vol. 25, no. 18, pp. 22055–22065, Sep. 2017.
[21] J. Li *et al*., "Full-band direct-conversion receiver with enhanced port isolation and I/Q phase balance using microwave photonic I/Q mixer," *Chin. Opt. Lett*, vol. 15, no. 1, Jan. 2017, Art. no. 010014.
[22] Z. Tang and S. Pan, "A reconfigurable photonic microwave mixer using a 90° optical hybrid," *IEEE Trans. Microw. Theory Techn*., vol. 64, no. 9, pp. 3017–3025, Sep. 2016.
[23] C. H. Huang *et al*., "Cascaded modulator topology for frequency conversion in antenna remoting applications," *Appl. Opt*., vol. 58, no. 9, pp. 2328–2333, Mar. 2019.
[24] V. R. Pagán and T. E. Murphy, "Electro-optic millimeter-wave harmonic downconversion and vector demodulation using cascaded phase modulation and optical filtering," *Opt. Lett*., vol. 40, no. 11, pp. 2481–2484, Jun. 2015.
[25] D. Shan *et al*., "Filter-free image-reject microwave photonic downconverter based on cascaded modulators," *Appl. Opt*., vol. 58, no. 13, pp. 3432–3437, May 2019.
[26] P. Li, W. Pan, X. Zou, B. Lu, L. Yan, and B. Luo, "Image-free microwave photonic down-conversion approach for fiber-optic antenna remoting," *IEEE J. Quantum Electron*., vol. 53, no. 4, pp. 1–8, Aug. 2017.
[27] B. Kang *et al*., "All-optical and broadband microwave image-reject receiver based on phase modulation and I/Q balanced detection," *J. Lightw. Technol*., vol. 38, no. 21, pp. 5962–5972, Nov. 2020.
[28] Z. Tu *et al*., "All-optical image-reject frequency down-conversion based on cascaded electro-optical modulators," *Opt. Commun*., vol. 430, pp. 158–162, Jan. 2019.
[29] M. Lei *et al*., "All-optical microwave I/Q mixer based on cascaded phase modulator and dual-drive Mach–Zehnder modulator," in *Proc. Opt. Fiber Commun. Conf*., 2019, pp. 1–3.